LAWRENCE
LIVERMORE
NATIONAL
LABORATORY

LLNL-JRNL-579193

High aspect ratio composite structures with 48.5% neutron efficiency

Q. Shao, L. F. Voss, A. M. Conway, R. P. Radev, R. J. Nikolic, M. A. Dar, C. L. Cheung

September 5, 2012

Applied Physics Letters

Disclaimer

High aspect ratio composite structures with 48.5% thermal neutron detection efficiency

Q. Shao,[1] L. F. Voss,[1] A. M. Conway,[1] R. J. Nikolic,[1, a)] M. A. Dar,[2] and C. L. Cheung[2]

[1]*Center for Micro and Nano Technology, Lawrence Livermore National Laboratory, 7000 East Avenue, Livermore, California 94550, USA*

[2]*Department of Chemistry, University of Nebraska–Lincoln, Lincoln, Nebraska 68588, USA*

The pillar structured thermal neutron detector is based on the combination of high aspect ratio silicon p-i-n pillars surrounded by the neutron converter material ^{10}B. By etching high aspect ratio pillar structures into silicon, the result is a device that efficiently absorbs the thermal neutron flux by accommodating a large volume fraction of ^{10}B within the silicon pillar array. Here, we report a thermal neutron detection efficiency of 48.5% using a 50 μm pillar array with an aspect ratio of 25:1.

Solid-state thermal neutron detectors are desired to replace the current ^{3}He tube based technology, which have issues with stability, sensitivity to microphonics and very recently a shortage of ^{3}He. There have been several semiconductor based thermal neutron detector design concepts developed including extensive work on lithium-6 fluoride and boron-10 carbide. Development of a compact semiconductor based thermal neutron detector requires an absorption material with a large cross section for the capture of thermal neutrons. Several isotopes are available: ^{6}Li, ^{10}B, ^{113}Cd, ^{155}Gd and ^{157}Gd, the most prominent of which are ^{6}Li, and ^{10}B.[1-13] The former must be used in a compound such as ^{6}LiF (Ref. 1, 2) due to the chemical instability of

[a)]Author to whom correspondence should be addressed. Email: nikolic1@llnl.gov

elemental Li, while the latter can be used in either its elemental form or in a compound, e.g. $^{10}B_5C$ (Ref. 14, 15), $^{10}B_4C$ (Ref. 16) and boron nitride[17]. The use of elemental ^{10}B is preferable because of its high thermal neutron cross section of 3840 barns.[18] A thickness of 50 μm will result in approximately 94% capture of the normally incident thermal neutrons. The compact thickness enables low power consumption by reducing the required operating voltage in the semiconductor detector.

Neutron capture by ^{10}B results in a nuclear reaction that releases a ^{7}Li and an α particle, which have ranges of 1.6 and 3.6 μm within the ^{10}B material respectively, for the most energetically favorable reaction. These distances are in conflict with the thickness of material required to efficiently capture incident thermal neutrons. Traditional semiconductor based detectors have consisted of a planar diode with a planar coating of neutron conversion material. This configuration has low detection efficiency, typically in the range of 2%-5%.[19] The design of an efficient semiconductor based thermal neutron detector must allow for a high probability of interaction between the semiconductor element and these by-products. Thus, 3D-structured semiconductors filled with thermal neutron absorbers have been developed to resolve the length scale conflicts.[3,6,20,21] The efficiency of perforated neutron detectors backfilled with ^{6}LiF was reported to be 29% at 10 volts reverse bias by Kansas State University.[22] A configuration consisting of back-to-back stacking of such devices has been reported to have 42% intrinsic thermal neutron efficiency operated at 3 volts reverse bias.[23-25] Similar silicon structures were investigated at Rensselaer Polytechnic Institute.[26-28] The reported intrinsic thermal neutron efficiencies were 4.5% based on natural boron (19.8% ^{10}B isotope) and 21% when scaled to 95% enriched ^{10}B . Our device design, shown in Figure 1, decouples the two length scales by etching high aspect ratio pillars into Si substrate followed by ^{10}B fill.[6] We previously reported detector

efficiency of 20% for 26 micron tall "pillar detectors".[13] By scaling the pillar height to 50 μm, a thermal neutron detection efficiency of 48.5% was obtained with a bias of zero volts.

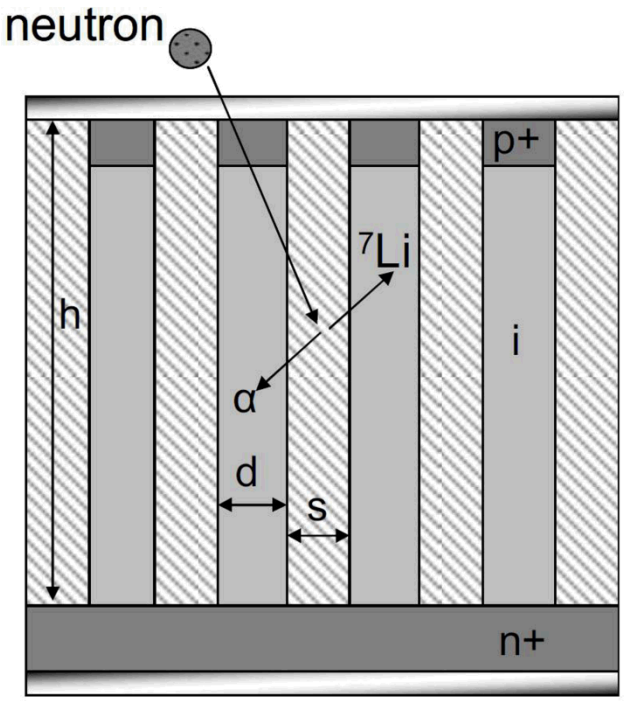

FIG. 1. Schematic of a pillar structured solid-state thermal neutron detector, d: pillar diameter (2 μm), s: pillar spacing (2 μm), h: pillar height (50 μm). (Ref. 6)

In the present work, a silicon wafer with structure of a 3 μm p^+ layer, a 47 μm intrinsic layer grown on an n^+ substrate was used for detector fabrication. The pillar diameter and spacing were defined lithographically, followed by inductively coupled plasma etching to form the pillar arrays as shown in Figure 2(a). The etched samples were then dipped into a nitric acid based silicon etching chemical to remove the plasma damaged silicon surface. A conformal ^{10}B coating by chemical vapor deposition (CVD) was deposited on the pillar arrays (Figure 2(b)). Bright field transmission electron microscopy (TEM) images (Figure 2(c)) show the interface between boron and silicon pillar. The surface roughness of the Si pillar is $R_a < \pm 26$ nm, where the red dot-

dash line is the reference surface. A smooth, defect and contamination free Silicon-Boron interface is desired for optimum charge collection. Plasma Quest electron cyclotron resonance (ECR) etching system was used for boron etching to expose the pillar tops, and metallization was done by sputtering Al/Cr/Au on the front side and backside of samples.

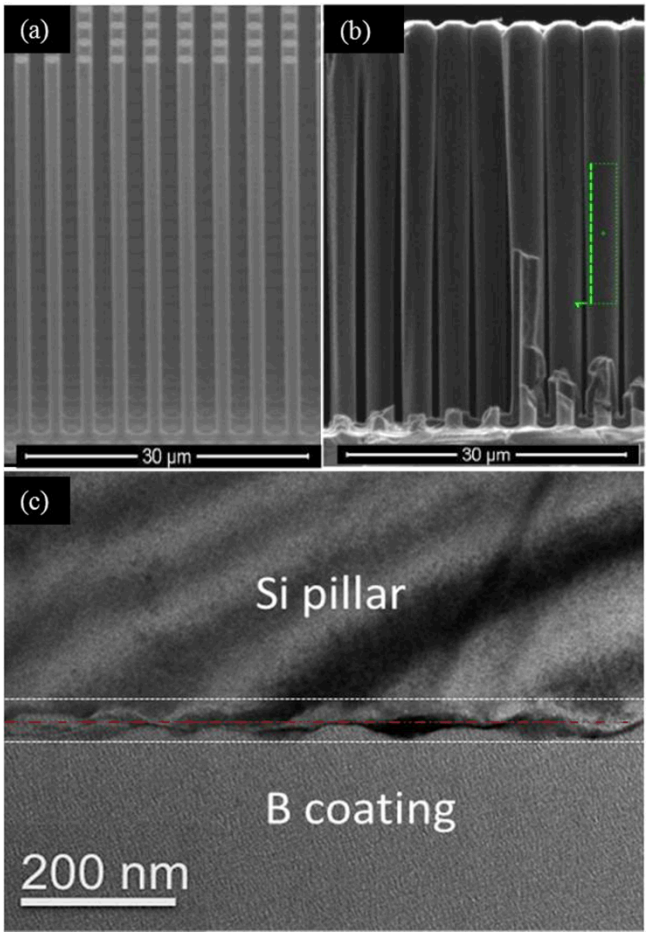

FIG. 2. Scanning electron microscopy (SEM) images of 50 µm silicon pillar structures: (a) as fabricated by etching, (b) after ^{10}B deposition, and the dotted box is showing the area where the sample was cut by Focused Ion Beam (FIB) for TEM analysis. (c) TEM image showing the roughness of Silicon-Boron interface.

The ^{10}B was deposited by CVD of $^{10}B_{10}H_{14}$. Depending on the precursor flux and the reaction pressure, the filling process can be controlled to favor the deposition of the ^{10}B on the

pillars due to the high sticking probability of the decomposed precursor onto the surface of the structured pillar substrates which results in a conformal coating instead of gas phase decomposition which would result in clogging at pillar surface.[29]

Optimizing the deposition temperature is critical; temperatures which are too low yield a high degree of fill and conformality of the ^{10}B film but an excess of hydrogen that leads to ^{10}B instability and the formation of H_3BO_3 crystallites as well as large amounts of film stress. Higher temperatures yield a ^{10}B film with excellent chemical stability and low stress but that does not uniformly coat the pillar structure. The chemical composition and stability of the ^{10}B coating on the pillar structured neutron detector samples were investigated by Fourier Transform Infrared Spectroscopy (FTIR). Stable amorphous boron films (no crystallite formation) were found on the samples with furnace set point temperature equal to or greater than 460 ^{o}C. There were no remarkable absorption peaks observed in FTIR spectra (upper graph in Figure 3(a)). At temperatures lower than 425 ^{o}C, crystallite formation was observed on samples after exposure to atmosphere. FTIR analysis identified these crystals as boric acid. Bands caused by complex O-H and B-O vibrations were found in the spectra (middle graph in Figure 3(a)) which are identical to what H_3BO_3 powder spectra showed (lower graph in Figure 3(a)).[30] Secondary-Ion Mass Spectrometry (SIMS) was used to study the hydrogen content in boron films which had not been exposed to atmosphere. The boron fill factors at varied deposition temperatures were analyzed by SEM (Figure 3(b), (c)). Note that the deposition time is the same for all samples with varied CVD temperatures. The boron films on top of pillar arrays were etched away by Reactive Ion Etching (RIE) to expose the silicon pillar tops. Figure 3(d) shows that both the hydrogen content in the boron film and the fill factor decrease with an increase in the deposition temperature. The high hydrogen content as measured by SIMS is attributed to incomplete decomposition of the

$B_{10}H_{14}$ precursor. The instability of the films deposited at low temperature is thus a result of excessive hydrogen. In addition to chemical stability and fill factor, stress from the B coating proves to be an issue. First, the shape of the pillars is critical. Any shape with corners results in concentrations of strain that are large enough to cause fracturing the Si pillars, as shown in the inset of Figure 3(e). A circular pillar structure overcomes this problem (Figure 3(e)). Second, the deposition time is important. Times which are too long lead to delamination of the ^{10}B film from the pillars as shown in Figure 3(f). In light of these considerations, an optimized deposition temperature profile of 460 °C was chosen for conformal ^{10}B coatings. It was also observed that with a pre-annealing of 900 °C for 15 minutes in flowing Ar prior to deposition was favorable for high quality amorphous boron films. These conditions provide stable B films of moderate stress and with acceptable fill factors.

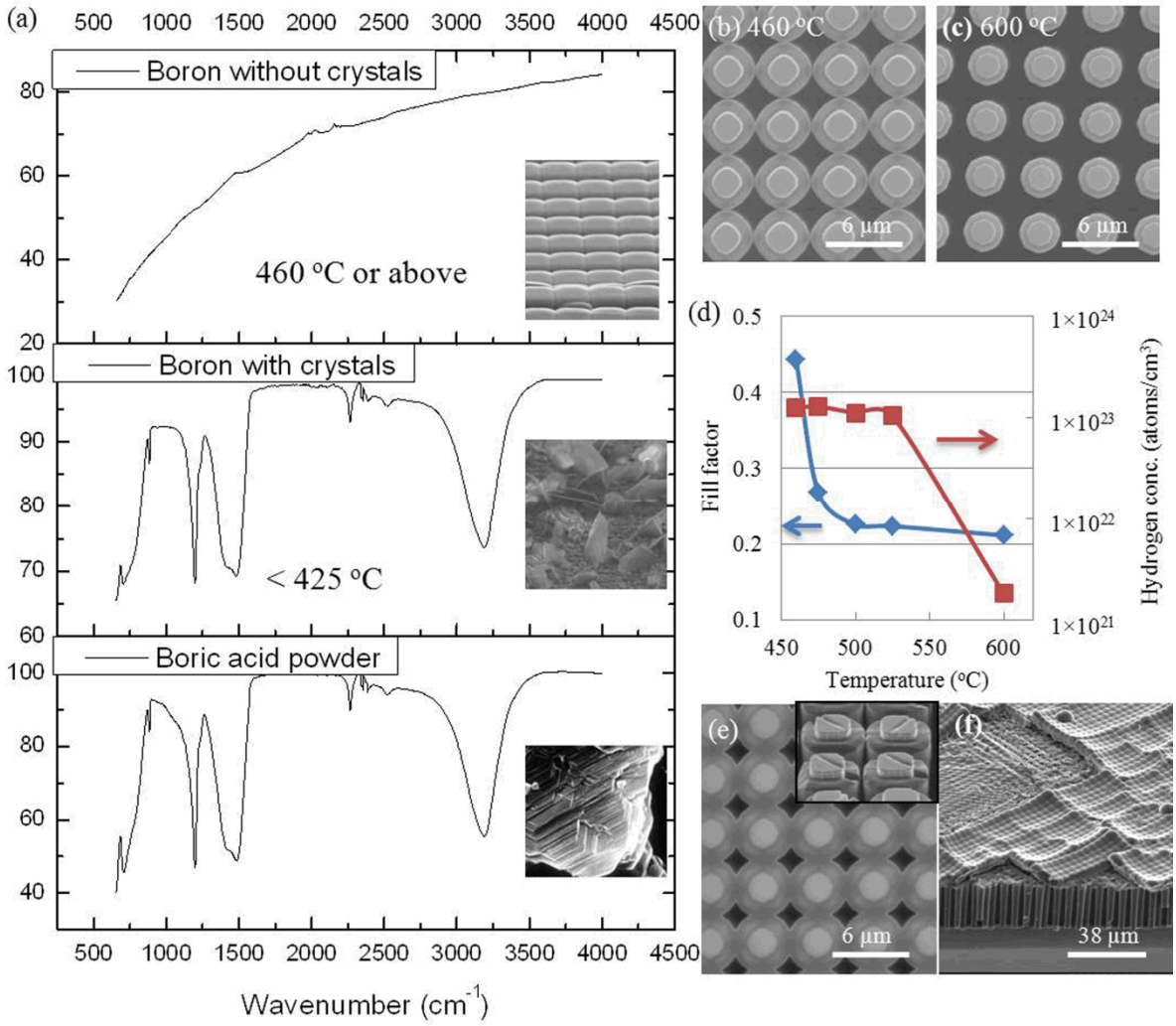

FIG. 3. Silicon pillar arrays filled with ^{10}B by CVD. (a) FTIR spectra of boron without crystals (upper), boron with crystals (middle) and boric acid powder (lower). The insets are the corresponding SEM images. (b) and (c) are SEM images (top view) of CVD boron with deposition temperature of 460 ^{o}C and 600 ^{o}C respectively. (d) Relation of boron fill factor, hydrogen concentration with boron deposition temperature. (e) SEM image (top view) of circular pillars surrounded by boron. Inset is showing the square pillars surrounded by boron. Indicated that the circular shape of silicon pillars effectively reduces or moderates stress which could occur

at the corners of square pillars. (f) SEM image of delaminated boron film on top of silicon pillar arrays due to excess deposition durations.

The neutron spectra of 2 × 2 mm^2, 50 μm tall pillar detectors were measured using a moderated ^{252}Cf source. The detectors were first mounted in a metal test assembly. Then high density polyethylene (HDPE) blocks were placed to surround the test box to thermalize the neutrons from a ^{252}Cf source which was placed on top of the HDPE blocks. The thermal neutron detection efficiencies were determined by comparing the neutron response of the device under test with a calibration pillar neutron detector with the same geometry. The calibration detector's efficiency was obtained in two ways. First its neutron response was compared with that of a 100% efficient ^{3}He tube using a collimated thermal neutron beam encompassing a "pin-hole" design with boric acid bricks for shielding and a HDPE moderated ^{252}Cf source. Second, the number of incident thermal neutrons was determined by Monte Carlo N-Particle (MCNP) simulations of the collimated configuration. The number of counts measured by the ^{3}He tube was found to agree within 5% with the number of neutrons simulated using MCNP.

In this paper we define the effective thermal neutron detection efficiency as the number of counted neutrons divided by the number of effective thermal neutrons incident on the detector, which was determined by modeling using MCNP and folding the simulated spectrum with the ^{10}B cross section. The effective thermal neutron flux is defined as follows:

$$\Phi(E_{thermal}) = \frac{1}{\sigma(E_{thermal})} \int_E \phi(E)\sigma(E)dE ,$$

where $\Phi(E_{thermal})$ is the integral effective thermal neutron flux, $\sigma(E_{thermal})$ is the thermal neutron cross section of ^{10}B, $\phi(E)$ is the energy dependent neutron flux, $\sigma(E)$ is the energy dependent

neutron cross section of ^{10}B. All detectors were measured under self-bias condition (0V). Increasing the detector bias will decrease capacitance, but increase leakage current. The pulse height spectrum is shown in Figure 4(a) together with a 26 µm pillar detector with 22% thermal neutron detection efficiency for comparison. The highest measured efficiency of the 50 µm detector is 48.5% with the low level discriminator (LLD) set to 30 keV which is above the noise floor energy. The measured efficiencies are in the range of 37% to 48.5% in one chip as shown in Figure 4 (b). The variation in the efficiency is likely due to temperature gradients in CVD during boron deposition, or non-uniform gas delivery to the substrate.

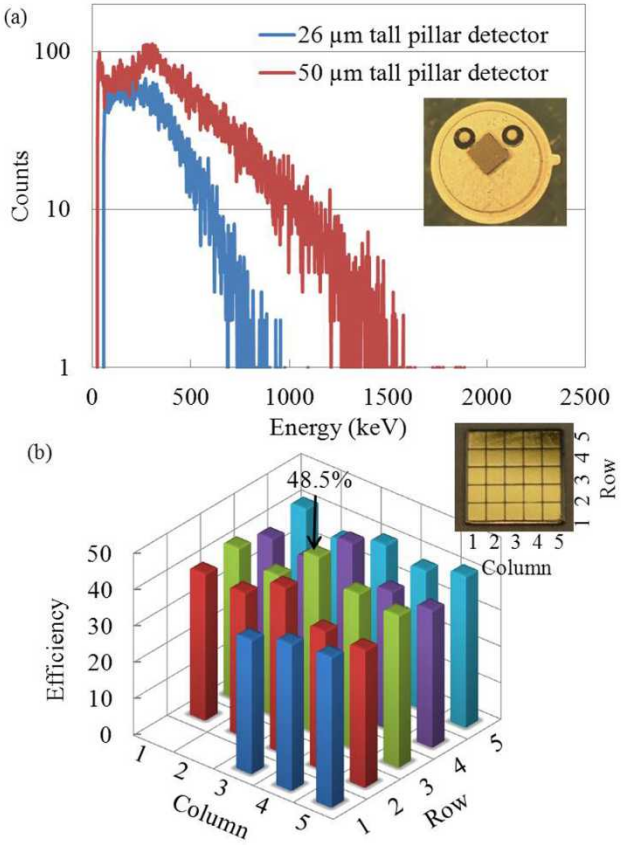

FIG. 4. Neutron radiation test on pillar structured thermal neutron detectors. (a) The comparison of measure neutron pulse height spectra of 26 µm and 50 µm tall pillar detectors. Inset is the

optical image of a detector (2 mm × 2 mm) wire bonded to a metal package. (b) The map of measured thermal neutron detection efficiencies on one 1.2 cm × 1.2 cm chip which has 25 detectors (2 mm × 2 mm) as shown in the inset.

In summary, we have demonstrated a composite structure design of the high aspect ratio silicon pillars integrated with conformal ^{10}B films for thermal neutron detection. The CVD ^{10}B films are developed and achieve an efficiency of 48.5% which is the highest reported efficiency for a semiconductor based thermal neutron detector.

The authors thank Catherine E. Reinhardt and Robert T. Graff for cleanroom processing support, Dr. Nick E. Teslich Jr for TEM sample preparation and Dr. Zurong Dai for TEM microscopy. The authors thank the Nebraska Center of Materials and Nanoscience and Center of Biotechnology for the use of their facilities. This work has been supported by the US Department of Homeland Security, Domestic Nuclear Detection Office, under competitively awarded IAA HSHQDC-07-X-00213. This support does not constitute an express or implied endorsement on the part of the Government. This work performed under the auspices of the U.S. Department of Energy by Lawrence Livermore National Laboratory under Contract DE-AC52-07NA27344, LLNL-JRNL-579193.

[1] W. J. McNeil, S. L. Bellinger, T. C. Unruh, E. L. Patterson, J. K. Shultis, and D. S. McGregor, IEEE Nucl. Sci. Symp. Conf. Rec. **6**, 3732-3735 (2006).

[2] D. S. McGregor, W. J. McNeil, S. L. Bellinger, T. C. Unruh, and J. K. Shultis, Nucl. Instr. and Meth. A **608**, 125-131 (2009).

[3] A. M. Conway, T. F. Wang, N. Deo, C. L. Cheung, and R. J. Nikolic, IEEE Trans. Nucl. Sci. **56**, 2802-2807 (2009).

[4] R. J. Nikolic, A. M. Conway, C. E. Reinhardt, R. T. Graff, T. F. Wang, N. Deo, and C. L. Cheung, 9th ICSICT, 2361-2364 (2008).

[5] R. J. Nikolic, C. L. Cheung, C. E. Reinhardt, and T. F. Wang, Proc. SPIE **6013**, 601305 (2005).

[6] R. J. Nikolic, A. M. Conway, C. E. Reinhardt, R. T. Graff, T. F. Wang, N. Deo, and C. L. Cheung, Appl. Phys. Lett. **93**, 133502 (2008).

[7] N. Deo, J. R. Brewer, C. E. Reinhardt, R. J. Nikolic, and C. L. Cheung, J. Vac. Sci. Technol. B **26**, 1309-1314 (2008).

[8] L. F. Voss, C. E. Reinhardt, R. T. Graff, A. M. Conway, R. J. Nikolic, N. Deo, and C. L. Cheung, Nucl. Instr. and Meth. A **606**, 821-823 (2009).

[9] L. F. Voss, C. E. Reinhardt, R. T. Graff, A. M. Conway, R. J. Nikolic, N. Deo, and C. L. Cheung, J. Electron. Mater. **39**, 263-267 (2010).

[10] L. F. Voss, Q. Shao, C. E. Reinhardt, R. T. Graff, A. M. Conway, R. J. Nikolic, N. Deo, and C. L. Cheung, J. Vac. Sci. Technol. B **28**, 916-920 (2010).

[11] Q. Shao, A. M. Conway, L. F. Voss, D. P. Heineck, C. E. Reinhardt, R. T. Graff, and R. J. Nikolic, ISDRS 1-2 (2009).

[12] Q. Shao, R. P. Radev, A. M. Conway, L. F. Voss, T. F. Wang, R. J. Nikolic, N. Deo, and C. L. Cheung, Proc. SPIE **8358**, 83581N (2012).

[13] R. J. Nikolic, A. M. Conway, R. Radev, Q. Shao, L. F. Voss, T. F. Wang, J. R. Brewer, C. L. Cheung, L. Fabris, C. L. Britton, and M. N. Ericson, Proc. SPIE **7805**, 78050O (2010).

[14] B. W. Robertson, S. Adenwalla, A. Harken, P. Weslch, J. I. Brand, P. A. Dowben, and J. P. Claasen, Appl. Phys. Lett. **80**, 3644 (2002).

[15]A. N. Caruso, P. A. Dowben, S. Balkir, N. Schemm, K. Osberg, R. W. Fairchild, O. B. Flores, S. Balaz, A. D. Harken, B. W. Robertson, and J. I. Brand, Mater. Sci. Eng. B **135**, 129-133 (2006).

[16]J. L. Lacy, A. Athanasiades, L. Sun, C. S. Martin, T. D. Lyons, M. A. Foss, and H. B. Haygood, Nucl. Instr. and Meth. A **652**, 359-363 (2011).

[17]J. Li, R. Dahal, S. Majety, J. Y. Lin, and H. X. Jiang, Nucl. Instr. and Meth. A **654**, 417-420 (2011).

[18]G. F. Knoll, Radiation Detection and Measurement, 3rd. ed. (Wiley, New York, 2000).

[19]D. S. McGregor, R. T. Klann, H. K. Gersch, and Y. H. Yang, Nucl. Instr. Meth. A **466**, 126 (2001).

[20]J. K. Shultis, and D. S. McGregor, IEEE Trans. Nucl. Sci. **53**, 1659-1665 (2006).

[21]D. S. McGregor, M. D. Hammig, H. K. Gersch, Y. -H. Yang, and R. T. Klann, Nucl. Instr. and Meth. A **500**, 272-308 (2003).

[22]D. S. McGregor, S. L. Bellinger, W. J. McNeil, and T. C. Unruh, IEEE Nucl. Sci. Symp. Conf. Rec. 446-448 (2008).

[23]S. L. Bellinger, R. G. Fronk, W. J. McNeil, T. J. Sobering, and D. S. McGregor, Nucl. Instr.and Meth. A **652**, 387-391 (2011).

[24]S. L. Bellinger, R. G. Fronk, T. J. Sobering, and D. S. McGregor, Appl. Radiat. Isotopes **70**, 1121-1124 (2012).

[25]S. L. Bellinger, R. G. Fronk, W. J. McNeil, T. J. Sobering, and D. S. McGregor, IEEE Trans. Nucl. Sci. **59**, 167-173 (2012).

[26]Y. Danon, J. Clinton, K. C. Huang, N. LiCausi, R. Dahal, J. -Q. Lu, and I. Bhat, JINST **7**, C03014 (2012).

[27]R. Dahal, K. C. Huang, J. Clinton, N. LiCausi, J. -Q. Lu, Y. Danon, and I. Bhat, Appl. Phys. Lett. **100**, 243507 (2012).

[28]K. C. Huang, R. Dahal, N. LiCausi, J. -Q. Lu, Y. Danon, and I. Bhat, J. Vac. Sci. Technol. B **30**, 051204 (2012).

[29]N. Deo, J. R. Brewer, C. E. Reinhardt, R. J. Nikolic, and C. L. Cheung, J. Vac. Sci. Technol. B **26**, 1309 (2008).

[30]E. F. Medvedev, and A. Sh. Komarevskaya, Glass and Ceramics **64**, 42-46 (2007).